Physics Letters B 837 (2023) 137639

Contents lists available at ScienceDirect

Physics Letters B

journal homepage: www.elsevier.com/locate/physletb

Probing the size and binding energy of the hypertriton in heavy ion collisions

C.A. Bertulani

Department of Physics and Astronomy, Texas A&M University-Commerce, TX 75429-3011, USA

ARTICLE INFO

Article history:
Received 22 November 2022
Received in revised form 17 December 2022
Accepted 17 December 2022
Available online 22 December 2022
Editor: B. Balantekin

ABSTRACT

The hypertriton is predicted to have a small binding energy (a weighted average of about 150 keV), consistent with a large matter radius (~ 10 fm), larger than the historical ^{11}Li halo discovered more than 35 years ago. But the reported experimental values of the binding energy of the hypertriton range from 70 to 400 keV. In this work I discuss the electromagnetic response and interaction radius of the hypertriton and how high energy heavy ion collisions ($\sim 1-2$ GeV/nucleon) can help achieving a higher accuracy for the determination of its size and binding energy.

1. Introduction

The equation of state (EOS) governing the structure of a neutron star (NS) is one of the main focuses of recent nuclear physics studies, invoking new theoretical methods, dedicated experiments at nuclear physics facilities, and astronomical observations with advanced telescopes and satellites [1]. The EOS is mainly ruled by the strong interaction within the neutron matter, but there is a consensus in the nuclear theory community that hyperons may appear in the inner core at about twice the nuclear saturation density (the nuclear saturation density is $\rho_0 = 0.16$ fm^{-3}) [2,3]. The presence of hyperons in the medium reduces the nucleonic Fermi energy and consequently the nuclear EOS is softened, limiting the mass that a NS can reach. This expectation has been challenged by the unexpected observation of NSs larger than twice the solar mass [4–7]. This conundrum has been termed as the "hyperon puzzle", although there are still some EOS that include hyperons but can still stabilize heavy NSs.

Key to understand the role of hyperons in NS is the hyperon-nucleon interaction. A plethora of nuclear experiments has been performed or are being planned to produce and study the properties of "hypernuclei", a term typically used for a Λ particle imbedded in a nucleus. Numerous properties of Λ-hypernuclei have been reported and compared to theoretical expectations. But none of these properties is more important than their binding energy. Its determination allows the theoretical adjustment of the Λ-nucleon interaction and to further predict other properties such as excitation energies, sizes and lifetimes. All these quantities, including the spins of light hypernuclei, are expected to be closely related [8,9], as observed in the case of halo nuclei [10].

The lightest observed hypernucleus is the hypertriton $^3_\Lambda$H, which has a large binding energy experimental uncertainty. Being the simplest of all hypernuclei, it is imperative to decrease this experimental uncertainty allowing for a more reliable description of heavier hypenuclei. A compilation of the $^3_\Lambda$H binding energy measurements is shown in Fig. 1, with data extracted from Refs. [11–18]. For simplicity, I assume that statistical and systematical errors are uncorrelated and added according to $\sigma^2 = \sigma^2_{stat} + \sigma^2_{sys}$. While Ref. [16] reports $B_\Lambda = 130 \pm 50$ keV, a recent STAR measurement obtained 410 ± 120 keV [18]. An ALICE experiment reported a much smaller value of 72^{+63}_{-36} keV [19]. The shaded band shown in Fig. 1 is the result of a statistical model analysis conducted in Ref. [20] for the average and uncertainty of the binding energies based on experimental errors and significant weights. The analysis of all existing data suggests that the Λ is bound to a deuteron by only 148 ± 40 keV.

The small binding energy in $^3_\Lambda$H implies that it has an extended wave function for the Λ with respect to the deuteron core, which has a much larger binding energy $B_d \simeq 2.2$ MeV. Thus the Λ forms a "halo" system with an approximate size $R = \sqrt{\hbar^2/(4\mu B_\Lambda)} \simeq 10$ fm, where μ is the reduced mass and B_Λ the hypertriton binding energy [21]. This is probably the largest known halo nucleus since the discovery of the ^{11}Li halo nucleus about 35 years ago [10].

The binding energy of the hypertriton is often used as a benchmark for the ΛN interaction, which is an important constraint in attempts to resolve the "hyperon puzzle" related to whether or not dense NSs contain hyperons, besides nucleons [1–3]. One has also been invoked a three-body ΛNN interaction together with a two-body interaction to study the hypertriton binding and other prop-

E-mail address: carlos.bertulani@tamuc.edu.

https://doi.org/10.1016/j.physletb.2022.137639

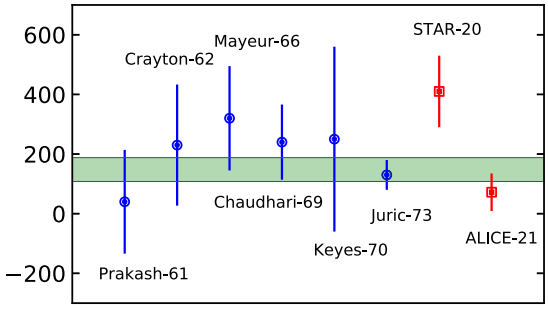

Fig. 1. Measurements of the binding energy of the hypertriton obtained with two-body and three-body pionic decays in emulsion and in heavy ion reaction experiments. The mean value was evaluated in Ref. [20] to be $B_\Lambda = 148 \pm 40$ keV (shaded band with statistical and total uncertainties).

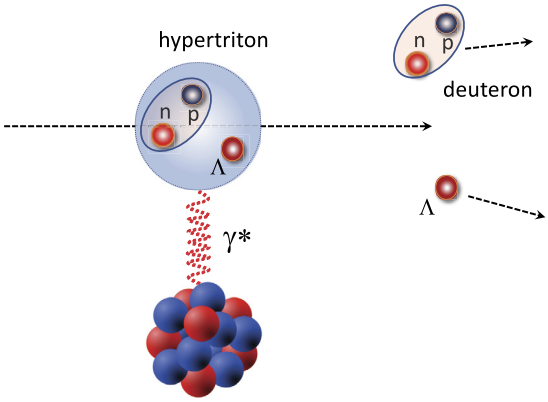

Fig. 2. Schematic view of the dissociation of the hypetriton in the Coulomb field of a nuclear target.

erties of hypernuclei [22,23]. The conclusion of these works is that the ΛNN interaction forces are not testable by studying the hypertriton. B_Λ is used in most YN studies to constrain the (S=1)/(S=0) ratio of the Λ-N 2-body force. Other studies have explored the details of the ΛN interaction using three-body models and effective field theoretical (EFT) techniques [24–26]. To further elucidate these questions, experimental studies of the hypertriton size and its corresponding binding energy have been proposed by measuring the interaction cross section of the hypertriton produced in reactions with heavy ion beams [27,28].

In this work, I explore how the hypertriton size and binding energy affects the magnitude of the electromagnetic breakup and interaction cross sections for hypertritons imping on carbon, tin and lead active targets (see Fig. 2). As a benchmark, I consider the reaction ${}^3_\Lambda$H + A → Λ + d + A at 1.5 GeV/nucleon with A = C, Sn and Pb targets. In particular, I show that the electromagnetic response of the hypertriton is very sensitive to its binding energy, yielding large breakup cross sections, comparable with the nuclear interaction cross sections. The electromagnetic response and the interaction cross section adds value to each other and can be complementarily used as standard probes of the binding energies and sizes of loosely-bound hypernuclei.

2. Theoretical framework

I will consider the general dependence of the electromagnetic response and interaction cross sections of the hypertriton with different target nuclei. At this time, there are no experiments to compare with and the exact details of the hypertriton wavefunction are only qualitatively relevant. I therefore adopt a simplified model for the structure of the hypertriton, treating it as a Λ particle bound to a deuteron by means of a Woods-Saxon (WS) potential. Similar models were proven very useful to understand the location of binding energies and single particle states in numerous hypernuclei along the periodic table [2,29].

For the electromagnetic breakup of the hypertriton in the active target I assume an electric dipole transition from the s-wave ground state ($l_0 = 0$) to the continuum. The transition $\gamma + {}^3_\Lambda\mathrm{H} \to d + \Lambda$, from the ground state (g.s.) of ${}^3_\Lambda$H to a continuum of $d + \Lambda$ with partial wave quantum numbers l, is considered. The bound-state wavefunctions are normalized to unity, $\int dr\,|u_0(r)|^2 = 1$, whereas the continuum wavefunctions for the Λ-d system have boundary conditions at infinity given by $-\sqrt{2\mu_{\Lambda d}/\pi\hbar^2 k}\, e^{i\delta_l} \sin(kr + \delta_l)$, where k is the wavenumber and δ_l is the partial wave phase-shift. With these definitions, the continuum wavefunctions are properly normalized as $\langle u_{E'}|u_E\rangle = \delta\left(E' - E\right)\delta_{ll'}$. The E1 operator will constrain transitions from the ground state to p-wave continuum states.

The multipole strength, or response function, for this system is given by [30]

$$\frac{dB(E1; g.s. \to El)}{dE} = \frac{1}{\hbar}\sqrt{\frac{\mu}{2E}}\,|\langle g.s.\|\mathcal{O}_{E1}\|El\rangle|^2, \tag{1}$$

where E is the relative kinetic energy of the Λ + deuteron, and $\langle g.s.\|\mathcal{O}_{E1}\|El\rangle$ is the dipole matrix element

$$\langle g.s.\|\mathcal{O}_{E1}\|El\rangle = (-1)^l \frac{e_{eff}}{\sqrt{4\pi}} \int_0^\infty dr\, r u_{g.s.}(r) u_E(r), \tag{2}$$

with $u_{g.s.}$ (u_E) being the ground-state (continuum) wavefunction, obtained from the solution of the radial Schrödinger equation, and the effective charge $e_{eff} = e(m_\Lambda/m_{{}^3_\Lambda\mathrm{H}})$ which accounts for the center-of-mass motion.

The virtual photons provided by the interaction of the target with the hypertriton will lead to its Coulomb dissociation, with the differential cross section

$$\frac{d\sigma_C}{dE} = \frac{16\pi^3}{9\hbar c} n(E) \frac{dB(E)}{dE}, \tag{3}$$

where the equivalent photon numbers are given by [31]

$$n(E) = \frac{2Z_T^2\alpha}{\pi}\left(\frac{Ec}{\gamma\hbar v^2}\right)^2 \int_0^\infty db\, b\left[K_1^2 + \frac{1}{\gamma^2}K_0^2\right] T(b), \tag{4}$$

with Z_T being the projectile charge, α the fine-structure constant, v the projectile (hypertriton) velocity, $\gamma = (1 - v^2/c^2)^{-1/2}$ is the Lorentz contraction and the modified Bessel functions K_n have the argument $x = Eb/\gamma\hbar v$.

The transparency function appearing in Eq. (4) accounts for absorption at small impact parameters, i.e., the probability that the hypertriton survives a collision with the target. It can be calculated using eikonal waves and the Glauber multiple scattering theory based on binary hadronic collisions. The transmission is a product of the survival probabilities of Λ, proton and neutron interacting with the target, i.e.,

$$T(b) = T_\Lambda(b) T_p(b) T_n(b), \tag{5}$$

where

$$T_i(b) = \int d^2 s_i\, dz_i\, \rho_i(z_i, \mathbf{s_i} - \mathbf{b}) \times \exp\left[-\sigma_{pi} Z_T \int dz'\, \rho_p^T(z', \mathbf{s})\right] \times \exp\left[-\sigma_{ni} N_T \int dz'\, \rho_n^T(z', \mathbf{s})\right], \tag{6}$$

Table I
Potential depths of the WS potential reproducing the hypertriton binding energy B_Λ.

B_Λ (keV)	100	150	200	300	500
V_0 [MeV]	-11.8	12.2	-12.6	-13.2	-14.3

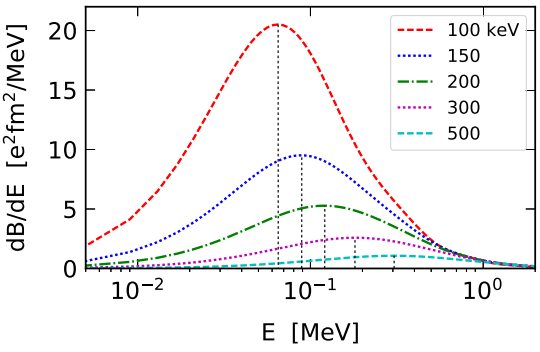

Fig. 3. Electric dipole response function, dB/dE, for ${}^3_\Lambda$H as a function of the relative kinetic energy of the final state of Λ-d. The calculations are performed for Λ-d separation energies B_Λ equal to 100, 150, 200, 300, and 500 keV. The vertical lines are analytical predictions for the maxima of the response functions from Ref. [33].

with $i = \Lambda$, p, or n, and all densities normalized to unity.

The proton and neutron densities in ${}^3_\Lambda$H are assumed to be the same and are obtained from a calculation for the deuteron wavefunction using the Av18 interaction [32]. The deuteron density is the outcome of an incoherent sum of the square of the S and D wavefunctions in its ground state. The proton and neutron densities within ${}^3_\Lambda$H are calculated from the free deuteron density, $\rho_d(\mathbf{r})$, obtained in this fashion. The proton and neutron densities are calculated with respect to the center of mass of the deuteron, where I assume equal neutron and proton masses, $m_p = m_n = m_N = 939$ MeV. For more details, see supplement.

The $\rho_\Lambda(\mathbf{r}_\Lambda)$ single-particle density is obtained from the square of the wavefunction resulting from the solution of the $\Lambda + d$ Schrödinger equation with the WS potential model described above. The neutron and Λ densities need to account for the center of mass displacement of the calculated wavefunctions. In the supplemental material I describe how the densities and S-matrices are calculated. After the center of mass corrections are performed, the nucleon and Λ densities are normalized to unity to comply with Eq. (6).

The total reaction cross section is given by the sum $\sigma_R = \sigma_C + \sigma_I$ of the Coulomb breakup cross section, $\sigma_C = \int dE\, d\sigma_C/dE$ and the "interaction cross section"

$$\sigma_I = 2\pi \int db\, b\,[1 - T(b)]\,. \tag{7}$$

3. Results

WS models have been used with success previously to reproduce binding energies and single particle states of hypernuclei yielding insights on their additional properties [2,29]. In this work, I calculate the bound state (s-wave) and continuum (p-wave) wavefunctions of the ${}^3_\Lambda$H system using a WS potential with parameters $R = 2.5$ fm (range) and $a = 0.65$ fm (difuseness). Its depth was adjusted to reproduce the Λ-d separation energy values B_Λ equal to 100, 150, 200, 300, and 500 keV. The depth and other parameters are taken to be the same for both the bound and continuum states. The potential depths are listed in Table I. The response functions dB/dE in units of e^2fm^2/MeV calculated with Eq. (1) are shown in Fig. 3 as a function of the relative kinetic energy of the fragments, E.

It is instructive to compare the numerical results for the response function obtained here with the analytical model developed in Ref. [33,34] using a Yukawa function for the bound-state wavefunction and a plane wave for the continuum. The model predicts a response function with an energy dependence [33,34]

$$\frac{dB}{dE} = \mathcal{C}\sqrt{B_\Lambda}\,\frac{E^{3/2}}{(E + B_\Lambda)^4}, \tag{8}$$

where B_Λ is the binding energy and $\mathcal{C}$ is a constant. The predicted maximum of this response function occurs at $E_{max} = 3B_\Lambda/5$. The location of these maxima is shown in Fig. 3 as vertical dotted lines and match perfectly the maxima of the calculated response functions using the WS model. The agreement is excellent for all binding energies shown in the figure. The shape of the response function is also very well reproduced with the analytical form of Eq. (8) with proper choices of the normalization constant $\mathcal{C}$. The differences are not larger than 4% for all binding energies considered here and low excitation energies, $E \lesssim 3B_\Lambda$.

The comparison with the analytical model of Eq. (8) implies that most details of the electromagnetic response of loosely bound systems are solely governed by the external part of the bound state wavefunction. It also means that the final state distortion through the interaction between the fragments Λ and d via the WS potential, included in the numerical calculation of the continuum waves, is rather small. The final state interaction of the fragments with the target nucleus has not been considered here, and is assumed to be small at GeV/nucleon bombarding energies. On the other hand, the magnitude and large energy tail of the response function is sensitive to some of the details of the bound state wavefunctions, such as the asymptotic normalization coefficients, and the numerical results are not quite reproduced by the analytical formula of Ref. [33]. Recent works have proved this assertion by using ab initio wavefunctions for light nuclei in the calculation of nuclear fragmentation observables [35,36].

In the final part of this manuscript I will discuss the numerical results for the interaction cross sections obtained for 1.5 GeV/nucleon ${}^3_\Lambda$H incident on ^{12}C, ^{120}Sn and ^{208}Pb targets. The calculations depend on the experimental values of the nucleon-nucleon and lambda-nucleon cross sections entering Eq. (6). I adopt the free pp and pn cross sections compiled by the particle data group [37], namely 45.8 mb and 40 mb, respectively. For the ΛN cross section I use $\sigma_{\Lambda N} = 35$ mb, consistent with the value reported in the literature [38,39]. The numerical results for the electromagnetic breakup (upper panel) and interaction (lower panel) cross sections are shown in Fig. 4. The shaded bands in the figure mark the one-sigma boundaries of the average value of hypertriton binding energy ($B_\Lambda = 148 \pm 40$ keV). Additionally, the numerical values for both fragmentation modes are presented in Table II as a function of the hypertriton binding energy B_Λ.

It is visible in Fig. 4 as well as in Table II that the Coulomb breakup cross sections for carbon targets are much smaller than the interaction cross sections. However, they increase rapidly with the charge of the projectile and for tin and lead targets they become comparable to the interaction cross sections. It is also worthwhile noticing that the Coulomb breakup cross section has a stronger dependence with the binding energy than the interaction cross section. The advantage of interaction cross sections is that they are relatively easy to measure. For a carbon target they imply a 12% reduction of the cross section σ_I from $B_\Lambda = 100$ MeV to $B_\Lambda = 500$ MeV. This sensitivity raises to 24% if one uses active lead targets. The sensitivity prospects increase dramatically in the Coulomb dissociation case, becoming 22% and 600%, respectively, for the same targets. The response function can be mapped experimentally by measuring the invariant mass of the fragments with the energies and momenta selection of the Λ and the deuteron.

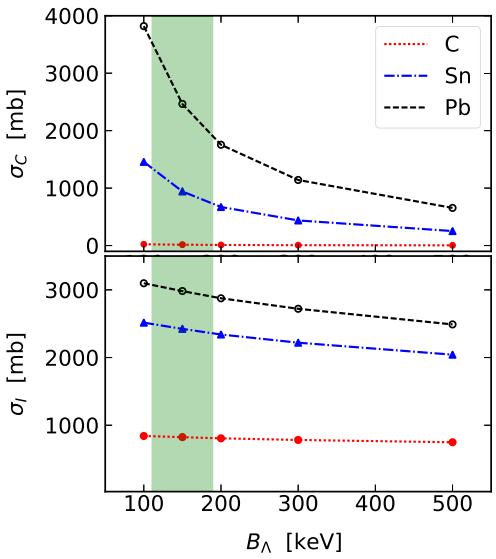

Fig. 4. *Upper panel.* Coulomb fragmentation cross section of 1.5 MeV/nucleon hypertriton projectiles impinging on carbon, tin and lead targets as a function of the hypertriton binding energy. *Lower panel.* Interaction cross section of 1.5 MeV/nucleon hypertriton projectiles incident on carbon, tin and lead targets as a function of the hypertriton binding energy. The shaded bands mark the one-sigma boundaries of the average value of hypertriton binding energy ($B_\Lambda = 148 \pm 40$ keV).

Table II
Coulomb breakup σ_C and interaction cross sections σ_I for the fragmentation of 1.5 GeV/nucleon ${}^{3}_{\Lambda}$H impinging on ^{12}C, ^{120}Sn and ^{208}Pb targets.

B_Λ (keV)	σ_C(C)	σ_C(Sn)	σ_C(Pb)	σ_I(C)	σ_I(Sn)	σ_I(Pb)
100	22.9	1457.	3820.	842.	2516.	3098.
150	14.9	942.	2464.	824.	2424.	2982.
200	10.7	672.	1755.	807.	2341.	2876.
300	7.1	438.	1142.	783.	2220.	2721.
500	4.1	253.	656.	749.	2043.	2490.

4. Conclusions

In this work I have considered the viability of using active targets to assess information on the binding energy of the hypertriton. These are important experiments, perhaps yielding precious information to help constrain theoretical models for the hypertriton.

I have used a simplified model for the hypertriton wavefunctions and densities because at the pre-experiment stage there is no need for a more elaborate calculation. The Glauber-reaction model is appropriate for the bombarding energy considered. The conclusions are that the electromagnetic response of the hypertriton is more sensitive to the binding energy than the interaction cross sections. By looking at inclusive quantities such as the reaction vertex, and invariant mass and momenta of the fragments, a mapping of the electrogmagnetic response of the hypertriton would be of great experimental and theoretical value for the hypernuclei research community, as it has been for the study of weakly-bound nuclei.

Declaration of competing interest

The authors declare that they have no known competing financial interests or personal relationships that could have appeared to influence the work reported in this paper.

Data availability

The data that has been used is confidential.

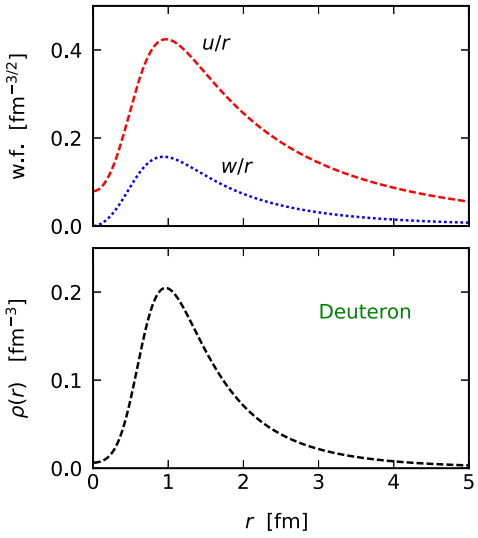

Fig. 5. *Upper panel:* Deuteron radial S-wave, $u(r)/r$, and D-wave, $w(r)/r$ wavefunctions. *Lower panel:* Deuteron density as a function of the proton-neutron distance r.

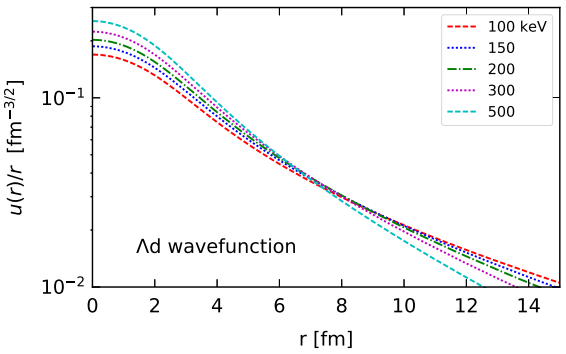

Fig. 6. Lambda-deuteron radial S-wave, $u_{\Lambda d}(r)/r$, as a function of the Λ-d distance r.

Acknowledgements

The author acknowledges support by the U.S. DOE grant DE-FG02-08ER41533 and the Helmholtz Research Academy Hesse for FAIR.

Appendix A

A.1. Deuteron and Λ-deuteron wavefunctions

The deuteron radial S-wave, $u(r)/r$, and D-wave, $w(r)/r$, wavefunctions and their densities are plotted in Fig. 5 as a function of the proton-neutron distance r. The wavefunctions have been calculated with the Av18 interaction [32] which fits the low energy pp and pn scattering data with great precision in the energy region 1-350 MeV.

The Λ-deuteron wavefunction is calculated using a Woods-Saxon (WS) potential with a radius parameter $R = 2.5$ fm and diffuseness $a = 0.65$ fm. The potential depth is chosen to reproduce the binding energy. The wavefunctions $u(r)/r$ for the S-wave are shown in Fig. 6 for binding energies $B_\Lambda = 100$, 150, 200, 300 and 500 keV.

A.2. Nucleon and Λ densities in the hypertriton

To calculate the nucleon and Λ coordinate distribution within in the hypertriton with the densities and wavefunctions described

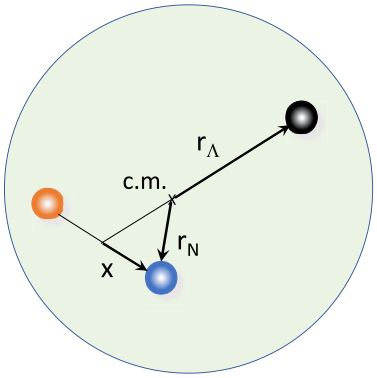

Fig. 7. Coordinates used in the text.

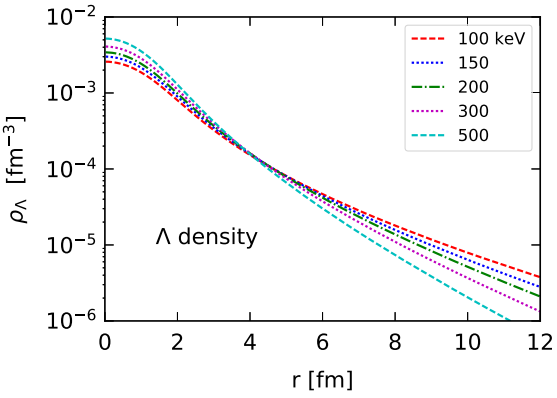

Fig. 8. Λ density as a function of the distance to the c.m. of the hypertriton.

above one needs to consider the center of mass correction. The center of mass of the system also needs to be considered when determining the nucleon densities, assumed to be the same for protons and neutrons. For clarity, I show in Fig. 7 the coordinates used in the following equations.

Defining the factors

$$\alpha = \frac{m_d}{(m_\Lambda + m_d)} \quad \text{and} \quad \beta = \frac{m_\Lambda}{(m_\Lambda + m_d)}, \tag{9}$$

the Λ density within the hypertriton as a function of its distance to the center of mass, **r**, is given by

$$\rho_\Lambda(\mathbf{r}) = |\Psi_{\Lambda d}(\mathbf{r}/\alpha)|^2, \tag{10}$$

with the previously calculated radial wavefunction $\Psi_{\Lambda d}(r_{\Lambda d}) = u_{\Lambda d}(r_{\Lambda d})/r_{\Lambda d}$. As required by the use of Eq. (6), the density $\rho_\Lambda(\mathbf{r})$ is subsequently normalized to unity.

To obtain the proton (neutron) density within the hypertriton we need to consider the probability to find the deuteron within the hypertriton multiplied by the probability to find the proton (neutron) within the deuteron. The former is given by $\rho_1(\mathbf{r}) = |\Psi_{\Lambda d}(\mathbf{r}/\beta)|^2$ and the later is given by $\rho_2(\mathbf{x}) = |\Psi_{deut}(2\mathbf{x})|^2$.

The nucleon density at position **r** within the nucleus is calculated with the convolution

$$\rho_N(\mathbf{r}) = \int d^3x \rho_1(|\mathbf{r} - \mathbf{x}|)\rho_2(\mathbf{x}). \tag{11}$$

This integral has cylindrical symmetry, requiring only two integrations. As with the case of the lambda density, the nucleon density $\rho_N(r)$ is normalized to unity, in accordance with Eq. (6).

Fig. 8 shows the density distribution of the Λ within the hypertriton as a function of its distance to the c.m. of the system. As expected for a S-wave, the density is peaked at small distances and

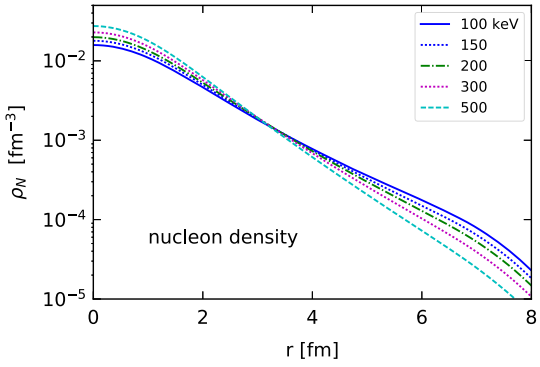

Fig. 9. Nucleon density as a function of the distance to the c.m. of the hypertriton.

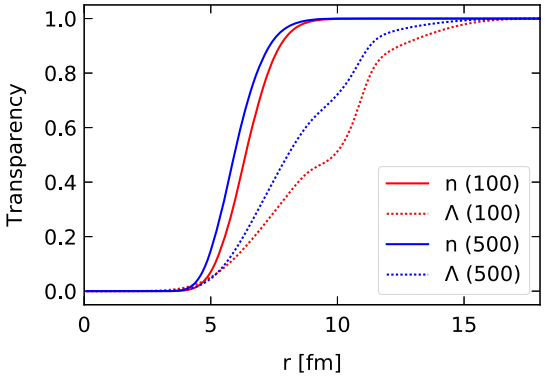

Fig. 10. Nucleon and lambda transparencies in a collision of a hypertriton and a carbon target nucleus at 1500 MeV/nucleon.

decays linearly at larges distances, with a larger slope for larger binding energy. The nucleon (proton or neutron) density in the hypertriton is displayed in Fig. 9 as a function of its distance to the c.m. of the system. A similar behavior is observed, as in the case of the Λ distribution. But in contrast to it, there is a shaper decrease of the nucleon distribution for large distances due to the stronger binding of the nucleons within the deuteron inside the hypertriton. At the center of the hypertriton, it is more likely to find a nucleon than the Λ particle by a factor of 10, as the Λ spreads out to much larger distances.

Once the particle densities are calculated, the transparency functions are obtained using Eq. (6). The numerical results are plotted in Fig. 10 for the nucleon and the lambda in a collision of a hypertriton and a carbon target at 1.5 GeV/nucleon. The transparency functions are straightforwardly related to the convolution of the distribution of each incident particle with that of nucleons inside the carbon target. The nucleon density overlap of the hypertriton nucleons and those within the carbon target decay fast with increasing impact parameter. The corresponding transparency for nucleon removal is different than zero for impact parameters that are roughly the sum of the root mean square radii of their distributions inside the hypertriton and the carbon. The same behavior is observed for the knockout of the Λ from the hypertriton at small impact parameters. However, the transition from full opaqueness to full transparency is not so abrupt and displays changes in the slope. The slope changes arise when the Λ density is sequentially probed from within the internal to the external part of the hypertriton where the Λ-deuteron wavefunction extends to large distances.

References

[1] J.M. Lattimer, Neutron stars and the nuclear matter equation of state, Annu. Rev. Nucl. Part. Sci. 71 (2021) 433–464.

[2] A. Gal, E.V. Hungerford, D.J. Millener, Strangeness in nuclear physics, Rev. Mod. Phys. 88 (2016) 035004.
[3] L. Tolos, L. Fabbietti, Strangeness in nuclei and neutron stars, Prog. Part. Nucl. Phys. 112 (2020) 103770.
[4] P.B. Demorest, T. Pennucci, S.M. Ransom, M.S.E. Roberts, J.W.T. Hessels, A two-solar-mass neutron star measured using Shapiro delay, Nature 467 (2010) 1081–1083.
[5] E.D. Barr, P.C.C. Freire, M. Kramer, D.J. Champion, M. Berezina, C.G. Bassa, A.G. Lyne, B.W. Stappers, A massive millisecond pulsar in an eccentric binary, Mon. Not. R. Astron. Soc. 465 (2016) 1711–1719.
[6] H.T. Cromartie, et al., Relativistic Shapiro delay measurements of an extremely massive millisecond pulsar, Nat. Astron. 4 (2020) 72–76.
[7] E. Fonseca, et al., Refined mass and geometric measurements of the high-mass PSR J0740+6620, Astrophys. J. Lett. 915 (2021) L12.
[8] R.H. Dalitz, G. Rajasekharan, The spins and lifetimes of the light hypernuclei, Phys. Lett. 1 (1962) 58–60.
[9] M. Rayet, R.H. Dalitz, The lifetime of 3HΛ, Nuovo Cimento A (1971-1996) 46 (1966) 786–794.
[10] I. Tanihata, H. Hamagaki, O. Hashimoto, Y. Shida, N. Yoshikawa, K. Sugimoto, O. Yamakawa, T. Kobayashi, N. Takahashi, Measurements of interaction cross sections and nuclear radii in the light p-shell region, Phys. Rev. Lett. 55 (1985) 2676–2679.
[11] Y. Prakash, P.H. Steinberg, D.A. Chandler, R.J. Prem, On the binding energies of mesic hypernuclei, Nuovo Cimento 21 (1961) 235–248.
[12] N. Crayton, R. Levi Setti, M. Raymund, O. Skjeggestad, D. Abeledo, R.G. Ammar, J.H. Roberts, E.N. Shipley, Compilation of hyperfragment binding energies, Rev. Mod. Phys. 34 (1962) 186–189.
[13] C. Mayeur, et al., A determination of the B_Λ values of light hypernuclei, Nuovo Cimento A (1965-1970) 43 (1966) 180.
[14] K.N. Chaudhari, S.N. Ganguli, N.K. Rao, M.S. Swami, A. Gurtu, J.M. Kohli, M.B. Singh, Binding energy and π^+ decay of light hyperfragments, Proc. Indian Acad. Sci., Sect. A 68 (1968) 228–243.
[15] G. Bohm, et al., A determination of the binding-energy values of light hypernuclei, Nucl. Phys. B 4 (1968) 511–526.
[16] M. Juric, et al., A new determination of the binding-energy values of the light hypernuclei ($A \leq 15$), Nucl. Phys. B 52 (1973) 1–30.
[17] D.H. Davis, 50 years of hypernuclear physics: I. the early experiments, Nucl. Phys. A 754 (2005) 3–13.
[18] J. Adam, et al., Measurement of the mass difference and the binding energy of the hypertriton and antihypertriton, Nat. Phys. 16 (2020) 409–412.
[19] ALICE Collaboration, Measurement of the lifetime and Λ separation energy of $^3_\Lambda$H, https://doi.org/10.48550/arxiv.2209.07360, 2022.
[20] Philipp Eckert, et al., Commissioning of the hypertriton binding energy measurement at MAMI, EPJ Web Conf. 271 (2022) 01006.
[21] C.A. Bertulani, L.F. Canto, M.S. Hussein, The structure and reactions of neutron-rich nuclei, Phys. Rep. 226 (1993) 281–376.
[22] Avraham Gal, Recent progress on hypernuclei, J. Phys. Conf. Ser. 1643 (2020) 012170.
[23] M. Kohno, H. Kamada, K. Miyagawa, Partial-wave expansion of λnn three-baryon interactions in chiral effective field theory, arXiv preprint, arXiv:2208.02388, 2022.
[24] A. Cobis, A.S. Jensen, D.V. Fedorov, The simplest strange three-body halo, J. Phys. G, Nucl. Part. Phys. 23 (1997) 401–421.
[25] F. Hildenbrand, H.-W. Hammer, Three-body hypernuclei in pionless effective field theory, Phys. Rev. C 100 (2019) 034002.
[26] E. Friedman, A. Gal, Constraints from Λ hypernuclei on the Λnn content of the Λ-nucleus potential and the 'hyperon puzzle', arXiv:2204.02264 [nucl-th], 2022.
[27] Peter Braun-Munzinger, Benjamin Dönigus, Loosely-bound objects produced in nuclear collisions at the LHC, Nucl. Phys. A 987 (2019) 144.
[28] A. Obertelli, et al., Matter radius of the hyperhalo candidate 3HΛ from interaction cross-section measurements, Proposal GSI-PAC, R3B collaboration, 2022.
[29] D.J. Millener, C.B. Dover, A. Gal, Λ-nucleus single-particle potentials, Phys. Rev. C 38 (1988) 2700–2708.
[30] C.A. Bertulani, 7Be(p,γ)8B cross section from indirect breakup experiments, Z. Phys. Hadrons Nucl. 356 (1996) 293–297.
[31] C.A. Bertulani, A.M. Nathan, Excitation and photon decay of giant resonances from high-energy collisions of heavy ions, Nucl. Phys. A 554 (1993) 158–172.
[32] R.B. Wiringa, V.G.J. Stoks, R. Schiavilla, Accurate nucleon-nucleon potential with charge-independence breaking, Phys. Rev. C 51 (1995) 38–51.
[33] C.A. Bertulani, A. Sustich, Multipole response of ^{11}Li, Phys. Rev. C 46 (1992) 2340–2343.
[34] C.A. Bertulani, G. Baur, Coincidence cross-sections for the dissociation of light-ions in high-energy collisions, Nucl. Phys. A 480 (1988) 615–628.
[35] C.A. Bertulani, A. Idini, C. Barbieri, Examination of the sensitivity of quasifree reactions to details of the bound-state overlap functions, Phys. Rev. C 104 (2021) L061602.
[36] Jianguo Li, Carlos A. Bertulani, Furong Xu, Nuclear spectroscopy with heavy ion nucleon knockout and (p, 2p) reactions, Phys. Rev. C 105 (2022) 024613.
[37] Particle Data Group, Review of particle physics, Prog. Theor. Exp. Phys. 2020 (2020), https://doi.org/10.1093/ptep/ptaa104.
[38] D. Bassano, C.Y. Chang, M. Goldberg, T. Kikuchi, J. Leitner, Lambda-proton interactions at high energies, Phys. Rev. 160 (1967) 1239–1244.
[39] S. Gjesdal, G. Presser, P. Steffen, J. Steinberger, F. Vannucci, H. Wahl, K. Kleinknecht, V. Lüth, G. Zech, A measurement of the total cross-sections for hyperon interactions on protons and neutrons in the momentum range from 6 GeV/c to 21 GeV/c, Phys. Lett. B 40 (1972) 152–156.